Oxic conditions in shallow marine settings during the Permian-Triassic Mass Extinction

Anja B. Frank[1], Elisabeth L. Warncke-Rüting[1], Stephen E. Grasby[2], Evelyn Kustatscher[3], Herwig Prinoth[4], Simon W. Poulton[5], Yijun Xiong[5], Dieter Korn[6], Jana Gliwa[7], William J. Foster[1]

[1] Universität Hamburg, Institut für Geologie; Hamburg, Germany.

[2] Geological Survey of Canada, Natural Resources Canada; Calgary, Alberta, Canada.

[3] Museum of Nature South Tyrol; Bozen/Bolzano, South Tyrol, Italy

[4] Museum Ladin; St. Martin in Thurn/San Martino in Badia, South Tyrol, Italy

[5] School of Earth and Environment, University of Leeds; Leeds, UK

[6] Museum für Naturkunde Berlin, Leibniz Institute for Evolution and Biodiversity Science; Berlin, Germany

[7] Freie Universität Berlin, Institut für Geologische Wissenschaften; Berlin, Germany

ABSTRACT

The concept that ultra-shallow marine anoxia was a major cause of the Permian-Triassic mass extinction was partly based on sections from the Dolomites (Italy). We test this hypothesis by re-examining the Dolomites record, utilizing an updated redox sensitive trace metal (V, U and Mo) approach, combined with Fe speciation and Th/U ratios, and paleontological observations.

23 Redox sensitive trace metal and Fe speciation data reveal fluctuating redox conditions prior to

24 the extinction, with periodic enrichments in highly reactive Fe likely reflecting Fe^{2+} mobilization

25 in anoxic ferruginous deeper waters. Oxic conditions are indicated during and after the extinction

26 event, suggesting that local redox conditions did not control biodiversity changes. However, this

27 redox reconstruction contrasts somewhat with traditional interpretation of Th/U ratios, which

28 indicate more persistent shallow water anoxia, likely due to a strong regional influence of the

29 detrital sediment composition. A comparison with other shallow marine successions reveals

30 similar redox trends, suggesting that shallow water anoxia was not global. Instead, redox

31 conditions across the Permian/Triassic boundary were likely variable, rendering it vital to assess

32 the role of anoxia on a site-specific basis to understand its role in the shallow marine Permian-

33 Triassic mass extinction.

34 **INTRODUCTION**

35   The Permian-Triassic mass extinction (PTME) marks the greatest loss of marine life in

36 the Phanerozoic, with > 90% of marine species going extinct (e.g., Erwin, 1993). Drastic

37 environmental changes associated with the emplacement of the Siberian Traps Large Igneous

38 Province have been proposed as the driving mechanisms behind the extinction (e.g., Grasby and

39 Bond, 2023; Svensen et al., 2023). The release of large volumes of greenhouse gases is

40 hypothesized to have led to a rapid rise in sea surface temperatures, ocean acidification, an

41 increased heavy metal supply, and a spread in ocean anoxia (e.g., Dal Corso et al., 2022; Grasby

42 and Bond, 2023). The expansion of oxygen minimum zones, leading to anoxic or euxinic

43 conditions even in shallow basins, was one of the first proposed extinction drivers (Twitchett and

44 Wignall, 1996; Wignall and Twitchett, 1996). Many subsequent studies have presented

45 supporting evidence for the development of such conditions during the extinction (Algeo et al.,

46 2007; Grice et al., 2005; Hays et al., 2007; Xiang et al., 2020; Zhang et al., 2020), rendering

47 anoxia a frequently cited driver of the marine extinction. However, in some places the event has

48 been suggested to occur under partially or completely oxic conditions (Algeo et al., 2010; Collin

49 et al., 2015; Foster et al., 2024; Gliwa et al., 2020; Knies et al., 2013; Loope et al., 2013;

50 Proemse et al., 2013; Yang et al., 2024), questioning the importance of anoxia as a global

51 extinction driver.

52   Considering these variable redox interpretations, it is vital to not only constrain changes

53 in local redox conditions, but also to link these changes to biodiversity changes at the same

54 location, to fully understand the potential role of oxygen availability in the extinction. To address

55 this, we examined the Seis section, a shallow marine Permian-Triassic sedimentary section from

56 the Dolomites, Italy. This is a key section that has been used to suggest that shallow marine

57 anoxia was a key driver of the extinction, based on Th/U ratios, the presence of opportunistic

58 taxa (lingulids and *Claraia*), and pyrite morphologies (Wignall and Twitchett, 1996). However,

59 only post-extinction data have been presented for the Seis section, speaking to a delayed

60 recovery processes, while the critical interval proceeding and during the extinction remain

61 unconstrained.

62   Currently, there is thus limited evidence for anoxia associated with the mass extinction in

63 the Dolomites, and further study of marine redox conditions prior to and during the event is

64 clearly warranted. To address this, we examined the pre-, during- and post-extinction strata of

65 Seis using redox sensitive trace metals (V, U and Mo), alongside Fe speciation and the

66 previously applied Th/U proxy. We then combine these data with lithological and available

67 paleontological data to test the hypothesis that anoxia was the main driver of the shallow marine

68 extinction in the western Tethys.

69 **STUDY AREA**

70   The studied section is located in the Dolomites, Italy, at 46.53374, 11.56142 (Fig. 1A)

71 and is known as the Siusi, Seis, Seis/Siusi or Seiser Klamm section (hereafter referred to as

72 Seis). Across the Permian/Triassic boundary (PTB), the Dolomites were part of the Adria

73 tectonic block located near the equator in the western Paleotethys. The Late Permian and Early

74 Triassic sedimentary successions of the Dolomites were deposited in a shallow marine basin on

75 the western margin of the Paleotethys as the Bellerophon and Werfen formations (Fig. 1B). The

76 Bellerophon Formation consists of fossiliferous limestones and dolostones, interbedded with

77 siltstones, sandstones and gypsum (Broglio Loriga et al., 1982; Farabegoli et al., 2007). The

78 overlying Werfen Formation is characterized by shallow marine limestones, dolostones,

79 siltstones and sandstones (Broglio Loriga et al., 1982; Farabegoli et al., 2007) and records the

80 PTME and PTB in its lowermost members (Farabegoli et al., 2007; Posenato, 2019).

81 **METHODS**

82 The Seis section was logged using the formation and unit/member definitions of Broglio Loriga

83 et al. (1982) with some amendments (Fig. 2). A total of 38 samples were taken and analyzed for

84 total organic carbon (TOC) as well as major and trace elements at the Geological Survey of

85 Canada, Calgary. We report redox sensitive trace metal (RSTM) concentrations in terms of

86 enrichment factors (EFs), using the revised method of Krewer et al. (2024) to account for

87 dilution of the detrital input by carbonate (termed EF^*). Additionally, iron speciation separation

88 was performed at the University of Leeds. The sum of the extracted Fe phases defines a highly

89 reactive Fe pool (Fe_{Hr}), which when normalized to total Fe (Fe_T) allows oxic conditions

90 ($Fe_{Hr}/Fe_T < 0.22$) to be distinguished from anoxic conditions ($Fe_{Hr}/Fe_T > 0.38$), with intermediate

91 ratios considered equivocal (Poulton and Canfield, 2011). For anoxic samples, pyrite Fe (Fe_{Py})

92   normalized to Fe_{Hr} further allow ferruginous conditions ($Fe_{Py}/Fe_{Hr} < 0.6$) to be distinguished

93   from euxinia ($Fe_{Py}/Fe_{Hr} > 0.8$), with ratios of 0.6-0.8 considered equivocal (Poulton, 2021). The

94   detailed sample preparation, digestion and analytical techniques as well as the complete

95   geochemical data set are given in the supplemental material[1].

RESULTS AND DISCUSSION

Redox evolution across the PTB

98   The carbonate-carbon isotope ($\delta^{13}C_{carb}$) record of Seis (Siegert et al., 2011) shows that the

99   negative $\delta^{13}C_{carb}$ excursion indicative of the global environmental perturbations in the Late

100   Permian coincided with the PTME (Fig. 3), supporting the importance of environmental change,

101   such as deoxygenation, for the event. Redox sensitive trace metal contents fluctuate, but

102   consistent patterns appear when the data are expressed as enrichment factors (Fig. 3). The $EF_V{}^*$

103   values generally fall close to the baseline of 1 throughout the section, but with a peak at ~2.75 m

104   that coincides with peaks in $EF_U{}^*$ and $EF_{Mo}{}^*$, indicating a particularly enhanced interval of

105   anoxia. A slight decrease in $EF_V{}^*$ values occurs at ~10.7 m, again consistent with the $EF_U{}^*$ and

106    $EF_{Mo}{}^*$ data, indicating a pronounced oxic interval and suggesting fluctuations in oxygenation

107   levels through the pre-extinction interval. Indeed, the $EF_U{}^*$ and $EF_{Mo}{}^*$ data, which tend to be

108   more sensitive redox proxies relative to V (see Li et al., 2025), suggest that redox conditions

109   were particularly dynamic during this interval, with regular fluctuations between oxic and anoxic

110   conditions (Fig. 3). This is supported by occasional spikes in TOC, as well as the presence of

111   thin, dark, fine-grained layers interbedded with the carbonates (Figs. 2, 3).

112   Intervals of elevated Fe_{Hr}/Fe_T with low Fe_{Py}/Fe_{Hr} ratios support periodic development of

113   anoxic ferruginous water column conditions in the pre-extinction phase, likely reflecting

114   mobilization of Fe^{2+} in deeper anoxic waters, followed by precipitation of Fe_{Hr} phases under oxic

115   or dysoxic conditions at the chemocline or following upwelling into oxic shallow waters.

116   Samples with very low Fe_T (< 0.5 wt%), which occur coincident with low TOC contents, have

117   also been suggested to represent oxic depositional conditions (Clarkson et al., 2014), thereby

118   supporting fluctuating redox conditions. These dynamics are further supported by EF_{Mn}^* values

119   (Fig. 3), which show pronounced peaks likely reflecting precipitation of water column Mn

120   during intervals of particularly enhanced shallow water oxygenation. We also note that Fe

121   speciation data reported for the GSSP in south China reveal a similar redox pattern, with large

122   gaps in the record and anoxic signatures leading up to the PTME, taken as evidence for fleeting

123   anoxia (Xiang et al., 2020).

124   During and after the extinction, however, the RSTM EF^* values persistently fall close to

125   1 (Fig. 3), suggesting prevailing oxic conditions. Initially low Fe_T contents (< 0.5 wt%) support

126   this interpretation, while a subsequent increase in Fe_{Hr}/Fe_T ratios and EF_{Mn}^* values in tandem,

127   suggests precipitation of reduced Fe and Mn under oxic water column conditions, hence

128   indicating upwelling of deeper anoxic waters into persistently oxic shallower waters.

129   The Th/U values at Seis (Fig. 3) provide conflicting redox results when considered

130   relative to traditional threshold value of 2, with lower values suggesting anoxia, while ratios of >

131   2 indicate oxia (Wignall and Twitchett, 1996). While the Th/U ratios shows a considerable

132   variability commonly coinciding with the other redox proxies, they are further highly correlated

133   to the detrital tracer Al (r = 0.71). The latter suggests that the redox control of the Th/U might be

134   partially masked by lithological change, emphasizing the advantage of utilizing EF* in sections

135   with variable detrital content.

136   Some of the intervals interpreted as being deposited under oxic conditions may in fact

137   reflect dysoxic deposition, since when considered in isolation, none of the applied redox proxies

138   can provide a robust distinction between these two redox states. To evaluate this, we consider an

139   EF_{Mo}^* versus EF_U^* cross-plot (Fig. 4; Tribovillard et al., 2012) in relation to redox trajectories

140   observed in modern redox sensitive marine environments (Li et al., 2025). The data do not

141   generally follow the redox trajectory, which marks the trend that modern dysoxic sediments tend

142   to fall on (Li et al., 2025). Instead, the majority of data plot either in the oxic zone or between the

143   particulate shuttle and redox trajectories, with the latter being typical of fully anoxic sediments

144   (Li et al., 2025). Specifically, the Casera Razzo Member and Ostracod Unit samples generally

145   record EF^* systematics typical of anoxic conditions, with the exception of some samples

146   indicative of oxic conditions, supporting redox fluctuations between oxic and fully anoxic. The

147   thin Bulla Member, which occurs just prior to the extinction horizon (see Fig. 2) and is

148   represented by only 1 sample, is somewhat anomalous, in that this sample plots close to the

149   redox trajectory, potentially indicating dysoxic conditions (Fig. 4). The overlying Tesero

150   (marking the PTME) and Mazzin members plot in the region typical of modern oxic sediments

151   (Li et al., 2025).

152   Taken together, our combined evaluation of multiple redox proxies challenges the

153   suggestion of a sharp swing to anoxic conditions at the beginning of the PTME (Wignall and

154   Twitchett, 1996).

155   **Redox and biodiversity changes**

156   The redox conditions at Seis were highly dynamic prior to the PTME, suggesting that the

157   late Permian ecosystem underwent significant oxygen stress. However, conditions appear to have

158   improved across the extinction horizon itself, questioning the role of anoxia as an extinction

159   trigger in very shallow waters. Further insight into the role of anoxia as an ecological stressor

160   may be gained by relating redox changes to the fossil record. While the redox proxy data support

161   reoccurring anoxia during deposition of the Casera Razzo Member (Figs. 3, 4), its diverse fossil

162   assemblage of algae, foraminifera, ostracods, mollusks and trace fossils (Fig. 2, Broglio Loriga et

163   al., 1988; Cirilli et al., 1998; Farabegoli et al., 2007; Mette and Roozbahani, 2012; Prinoth and

164   Posenato, 2023; Twitchett and Wignall, 1996) required an oxygenated environment. Hence, the

165   anoxic episodes were likely too short-lived to cause long-term uninhabitable conditions.

166   Similarly, the presence of ostracods, bivalves, gastropods and relatively large trace fossils in the

167   Ostracod Unit, as well as bioturbated beds and foraminifera in the Bulla Member (Broglio Loriga

168   et al., 1982; Cirilli et al., 1998; Crasquin et al., 2008; Farabegoli et al., 2007; Foster et al., 2017;

169   Groves et al., 2007; Mette and Roozbahani, 2012), suggest that episodic deoxygenation was not

170   widespread enough to severely impact biodiversity. Since the Ostracod Unit and Bulla Member

171   generally record lower RSTM EF[*] values compared to the underlying Casera Razzo Member

172   (Fig. 3), redox conditions and overall stability may have improved leading up to the PTME,

173   questioning the role of anoxia as an extinction cause in this setting.

174   **Role of anoxia as driver of shallow marine extinction during the PTME**

175   Many studies on the PTME present environmental changes identified at one location as a

176   potential global extinction mechanism. However, such an approach may fail to capture spatial

177   heterogeneity in extinction drivers between different water depths, ecosystems and regions.

178   Uranium isotope data suggest a global intensification of anoxia concurrent with the PTME

179   (Zhang et al., 2020), supported by many sections worldwide. However, the local geochemical

180   signatures at Seis are not consistent with a spread of anoxic waters into shallow waters at this

181   location, suggesting the presence of habitable zones in the western Tethys, which agrees well

182   with previous work from Panthalassa (Algeo et al., 2010; Beatty et al., 2008; Proemse et al.,

183   2013). Considering that the majority of marine fossils preserved in the rock record are found in

184 shallow marine settings, our knowledge of the PTME is mainly based on fossil data from such

185 settings. Hence, if anoxia did not impinge on the shallow western Tethys, it was not the cause of

186 the abrupt disappearance of fossils in this region.

187 While this might rule out anoxia as the main driver of the PTME in the shallow, western

188 Tethys, deoxygenation could still have been an extinction mechanism elsewhere. Redox

189 evaluations for the eastern Tethys yield heterogenous redox interpretations, but generally support

190 the development of at least episodic deoxygenation (Algeo et al., 2007; Xiang et al., 2020; Yang

191 et al., 2024). However, a recent meta-analysis of available geochemical and fossil data for the

192 GSSP in south China has revealed that temperature rise and nutrient stress were the driving

193 factors of the extinction there, while the role of anoxia has been considered ambiguous (Foster et

194 al., 2024). For the Neotethys, multiple studies have found no evidence for the development of

195 anoxic conditions within shallow carbonate platforms (Collin et al., 2015; Gliwa et al., 2020;

196 Loope et al., 2013). Finally, redox interpretations for Panthalassa support the prevalence of oxic

197 conditions as well as the development of anoxia (Algeo et al., 2010; Grice et al., 2005; Hays et

198 al., 2007; Knies et al., 2013; Proemse et al., 2013). Hence, the timing and degree of

199 deoxygenation was geographically variable, emphasizing that anoxia alone may not have been

200 responsible for the widespread extinction of life in shallow marine basins during the PTME.

201 **ACKNOWLEDGMENTS**

205 **REFERENCES CITED**

206 Algeo, T.J., Ellwood, B., Nguyen, T.K.T., Rowe, H., Maynard, J.B., 2007. The Permian–Triassic

207 boundary at Nhi Tao, Vietnam: Evidence for recurrent influx of sulfidic watermasses to a

208   shallow-marine carbonate platform. Palaeogeography, Palaeoclimatology, Palaeoecology,

209   The Permian-Triassic Boundary Crisis and Early Triassic Biotic Recovery 252, 304–327.

210   https://doi.org/10.1016/j.palaeo.2006.11.055

211 Algeo, T.J., Hinnov, L., Moser, J., Maynard, J.B., Elswick, E., Kuwahara, K., Sano, H., 2010.

212   Changes in productivity and redox conditions in the Panthalassic Ocean during the latest

213   Permian. Geology 38, 187–190. https://doi.org/10.1130/G30483.1

214 Beatty, T.W., Zonneveld, J.-P., Henderson, C.M., 2008. Anomalously diverse Early Triassic

215   ichnofossil assemblages in northwest Pangea: A case for a shallow-marine habitable

216   zone. Geology 36, 771–774. https://doi.org/10.1130/G24952A.1

217 Broglio Loriga, C., Masetti, D., Neri, C., 1982. La Formazione di Werfen (Scitico) delle

218   Dolomiti occidentali: sedimentologia e biostratigrafia. Associato all'Unione stampa

219   periodica italiana, Milano, Italie.

220 Broglio Loriga, C., Neri, C., Pasini, M., Posenato, R., 1988. Marine fossil assemblages from

221   Upper Permian to lowermost Triassic in the western Dolomites (Italy). Memorie di

222   Scienze Geologiche 34, 5–44.

223 Cirilli, S., Pirini Radrizzani, C., Ponton, M., Radrizzani, S., 1998. Stratigraphical and

224   palaeoenvironmental analysis of the Permian-Triassic transition in the Badia Valley

225   (Souther Alps, Italy). Palaeogeography, Palaeoclimatology, Palaeoecology 138, 85–113.

226   https://doi.org/10.1016/S0031-0182(97)00123-5

227 Collin, P.Y., Kershaw, S., Tribovillard, N., Forel, M.B., Crasquin, S., 2015. Geochemistry of

228   post-extinction microbialites as a powerful tool to assess the oxygenation of shallow

229   marine water in the immediate aftermath of the end-Permian mass extinction. Int J Earth

230   Sci (Geol Rundsch) 104, 1025–1037. https://doi.org/10.1007/s00531-014-1125-3

231 Crasquin, S., Perri, M.C., Nicora, A., Wever, P.D., 2008. Ostracods across the Permian-Triassic

232   boundary in Western Tethys: The Bulla parastratotype (Southern Alps, Italy). Rivista

233   italiana di Paleontologia e Stratigrafia Vol 114, No 2. https://doi.org/10.13130/2039-

234   4942/5900

235 Dal Corso, J., Song, H., Callegaro, S., Chu, D., Sun, Y., Hilton, J., Grasby, S.E., Joachimski,

236   M.M., Wignall, P.B., 2022. Environmental crises at the Permian–Triassic mass

237   extinction. Nat Rev Earth Environ 3, 197–214. https://doi.org/10.1038/s43017-021-

238   00259-4

239   Erwin, D.H., 1993. The Great Paleozoic Crisis: Life and Death in the Permian. Columbia
240   University Press.
241   Farabegoli, E., Perri, M.C., Posenato, R., 2007. Environmental and biotic changes across the
242   Permian–Triassic boundary in western Tethys: The Bulla parastratotype, Italy. Global
243   and Planetary Change, Environmental and Biotic Changes during the Paleozoic-Mesozoic
244   Transition 55, 109–135. https://doi.org/10.1016/j.gloplacha.2006.06.009
245   Foster, W.J., Danise, S., Price, G.D., Twitchett, R.J., 2017. Subsequent biotic crises delayed
246   marine recovery following the late Permian mass extinction event in northern Italy.
247   PLOS ONE 12, e0172321. https://doi.org/10.1371/journal.pone.0172321
248   Foster, W.J., Frank, A.B., Li, Q., Danise, S., Wang, X., Peckmann, J., 2024. Thermal and
249   nutrient stress drove Permian-Triassic shallow marine extinctions. Cambridge Prisms:
250   Extinction 1–25. https://doi.org/10.1017/ext.2024.9
251   Gliwa, J., Ghaderi, A., Leda, L., Schobben, M., Tomás, S., Foster, W.J., Forel, M.-B.,
252   Ghanizadeh Tabrizi, N., Grasby, S.E., Struck, U., Ashouri, A.R., Korn, D., 2020. Aras
253   Valley (northwest Iran): high-resolution stratigraphy of a continuous central Tethyan
254   Permian–Triassic boundary section. Fossil Record 23, 33–69. https://doi.org/10.5194/fr-
255   23-33-2020
256   Grasby, S.E., Bond, D.P.G., 2023. How Large Igneous Provinces Have Killed Most Life on
257   Earth—Numerous Times. Elements 19, 276–281.
258   https://doi.org/10.2138/gselements.19.5.276
259   Grice, K., Cao, C., Love, G.D., Böttcher, M.E., Twitchett, R.J., Grosjean, E., Summons, R.E.,
260   Turgeon, S.C., Dunning, W., Jin, Y., 2005. Photic Zone Euxinia During the Permian-
261   Triassic Superanoxic Event. Science. https://doi.org/10.1126/science.1104323
262   Groves, J.R., Rettori, R., Payne, J.L., Boyce, M.D., Altiner, D., 2007. End-Permian Mass
263   Extinction of Lagenide Foraminifers in the Southern Alps (Northern Italy). Journal of
264   Paleontology 81, 415–434.
265   Hays, L.E., Beatty, T., Henderson, C.M., Love, G.D., Summons, R.E., 2007. Evidence for photic
266   zone euxinia through the end-Permian mass extinction in the Panthalassic Ocean (Peace
267   River Basin, Western Canada). Palaeoworld, Contributions to Permian and Carboniferous
268   Stratigraphy, Brachiopod Palaeontology and End-Permian Mass Extinctions, In Memory
269   of Professor Yu-Gan Jin 16, 39–50. https://doi.org/10.1016/j.palwor.2007.05.008

270 Knies, J., Grasby, S.E., Beauchamp, B., Schubert, C.J., 2013. Water mass denitrification during
271   the latest Permian extinction in the Sverdrup Basin, Arctic Canada. Geology 41, 167–
272   170. https://doi.org/10.1130/G33816.1

273 Krewer, C., Poulton, S.W., Newton, R.J., März, C., Mills, B.J.W., Wagner, T., 2024. Controls on
274   the Termination of Cretaceous Oceanic Anoxic Event 2 in the Tarfaya Basin, Morocco.
275   American Journal of Science 324. https://doi.org/10.2475/001c.118797

276 Li, S., Wignall, P.B., Poulton, S.W., 2025. Co-application of rhenium, vanadium, uranium and
277   molybdenum as paleo-redox proxies: Insight from modern and ancient environments.
278   Chemical Geology 674, 122565. https://doi.org/10.1016/j.chemgeo.2024.122565

279 Loope, G.R., Kump, L.R., Arthur, M.A., 2013. Shallow water redox conditions from the
280   Permian–Triassic boundary microbialite: The rare earth element and iodine geochemistry
281   of carbonates from Turkey and South China. Chemical Geology 351, 195–208.
282   https://doi.org/10.1016/j.chemgeo.2013.05.014

283 Mette, W., Roozbahani, P., 2012. Late Permian (Changsingian) ostracods of the Bellerophon
284   Formation at Seis (Siusi) (Dolomites, Italy). Journal of Micropalaeontology 31, 73–87.
285   https://doi.org/10.1144/0262-821X11-010

286 Posenato, R., 2019. The end-Permian mass extinction (EPME) and the Early Triassic biotic
287   recovery in the western Dolomites (Italy): state of the art. Bollettino della Società
288   Paleontologica Italiana 11–34. https://doi.org/10.4435/BSPI.2019.05

289 Poulton, S.W., Canfield, D.E., 2011. Ferruginous Conditions: A Dominant Feature of the Ocean
290   through Earth's History. Elements 7, 107–112.
291   https://doi.org/10.2113/gselements.7.2.107

292 Prinoth, H., Posenato, R., 2023. Bivalves from the Changhsingian (upper Permian) Bellerophon
293   Formation of the Dolomites (Italy): ancestors of Lower Triassic post-extinction benthic
294   communities. Papers in Palaeontology 9, e1486. https://doi.org/10.1002/spp2.1486

295 Proemse, B.C., Grasby, S.E., Wieser, M.E., Mayer, B., Beauchamp, B., 2013. Molybdenum
296   isotopic evidence for oxic marine conditions during the latest Permian extinction.
297   Geology 41, 967–970. https://doi.org/10.1130/G34466.1

298 Siegert, S., Kraus, S.H., Mette, W., Struck, U., Korte, C., 2011. Organic carbon isotope values
299   from the Late Permian Seis/Siusi succession (Dolomites, Italy): Implications for

300   palaeoenvironmental changes. Fossil Record 14, 207–217.

301   https://doi.org/10.1002/mmng.201100008

302 Svensen, H.H., Jones, M.T., Mather, T.A., 2023. Large Igneous Provinces and the Release of

303   Thermogenic Volatiles from Sedimentary Basins. Elements 19, 282–288.

304   https://doi.org/10.2138/gselements.19.5.282

305 Tribovillard, N., Algeo, T.J., Baudin, F., Riboulleau, A., 2012. Analysis of marine environmental

306   conditions based onmolybdenum–uranium covariation—Applications to Mesozoic

307   paleoceanography. Chemical Geology, Special Issue Recent Advances in Trace Metal

308   Applications to Paleoceanographic Studies 324–325, 46–58.

309   https://doi.org/10.1016/j.chemgeo.2011.09.009

310 Twitchett, R.J., Wignall, P.B., 1996. Trace fossils and the aftermath of the Permo-Triassic mass

311   extinction: evidence from northern Italy. Palaeogeography, Palaeoclimatology,

312   Palaeoecology 124, 137–151. https://doi.org/10.1016/0031-0182(96)00008-9

313 Wignall, P.B., Twitchett, R.J., 1996. Oceanic Anoxia and the End Permian Mass Extinction.

314   Science 272, 1155–1158. https://doi.org/10.1126/science.272.5265.1155

315 Xiang, L., Zhang, H., Schoepfer, S.D., Cao, C., Zheng, Q., Yuan, D., Cai, Y., Shen, S., 2020.

316   Oceanic redox evolution around the end-Permian mass extinction at Meishan, South

317   China. Palaeogeography, Palaeoclimatology, Palaeoecology 544, 109626.

318   https://doi.org/10.1016/j.palaeo.2020.109626

319 Yang, F., Li, S., An, K.Y., Bond, D.P.G., Ao, R., Wu, X.B., Ma, L.L., Sun, Y.D., 2024. Re-

320   Evaluating Water Column Reoxygenation During the End Permian Mass Extinction.

321   Geochemistry, Geophysics, Geosystems 25, e2024GC011779.

322   https://doi.org/10.1029/2024GC011779

323 Zhang, F., Shen, S., Cui, Y., Lenton, T.M., Dahl, T.W., Zhang, H., Zheng, Q., Wang, W.,

324   Krainer, K., Anbar, A.D., 2020. Two distinct episodes of marine anoxia during the

325   Permian-Triassic crisis evidenced by uranium isotopes in marine dolostones. Geochimica

326   et Cosmochimica Acta, New developments in geochemical proxies for paleoceanographic

327   research 287, 165–179. https://doi.org/10.1016/j.gca.2020.01.032

328

329 FIGURE CAPTIONS

330 **Fig. 1 (A)** Paleogeographic map (WGS84) of the study area showing the location of Seis

331 outlining the emerged land (yellow), marine environment (blue) and Periadriatic lineament (red

332 line) (modified from Posenato, 2019). **(B)** Photograph of Seis, with the formation boundary

333 marked in red. People for scale.

334 **Fig. 2** Log of the Seis section, including paleontological observations made in the field. The

335 colors reflect the rock color and the red band marks the PTME (following Farabegoli et al.,

336 2007). The abbreviations m, w, p and g stand for mud-, wack-, pack- and grainstone,

337 respectively, and OU, B and T for Ostracod Unit, Bulla Member and Tesero Member,

338 respectively.

339 **Fig. 3** Trends in $\delta^{13}C_{Carb}$ (Siegert et al., 2011), RSM EF*, Fe speciation (black arrows marking

340 samples with iron <0.5wt%) and Th/U (Wignall and Twitchett, 1996 & this study) plotted next to

341 the log of Seis. Gray circles mark published data, the vertical gray dashed lines represent no

342 enrichment compared to PAAS, and the red dashed box marks the PTME.

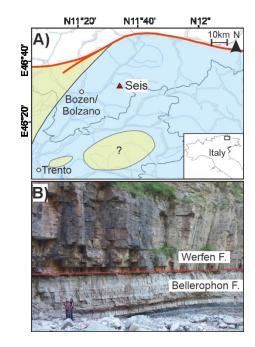343 **Fig. 4** Comparison of EF_U* to EF_{Mo}*. The red arrows indicate different Mo accumulation

344 pathways, with the redox variation trajectory illustrating benthic deoxygenation from oxic,

345 throgh dysoxic and anoxic, to euxinic conditions and the particle shuttle (PS) the uptake of Mo

346 through redox cycling of oxyhydroxides (Tribovillard et al., 2012). The diagonal dotted lines

347 represent proportions of the seawater (SW) Mo/U molar ratio.

348 [1]Supplemental Material. *Detailed methods description (S1.docx) and complete geochemical data*

349 *set (S2.xlsx).* Please visit https://doi.org/10.1130/XXXX to access the supplemental material, and

350 contact editing@geosociety.org with any questions.

351

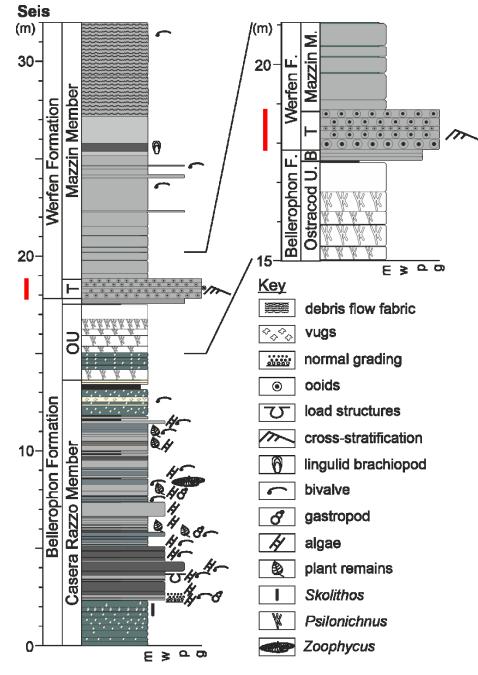352   FIGURES

353

354   **Fig. 2**

355

Fig. 2

356

357

359   **Fig. 3**

360

361

362   **Fig. 4**

363